Pyrimidine Derivatives with Terminal Pyridyl Heterocycles: Facile Synthesis and Their Antiproliferative Activities

Khushwant Singh,[a] Achintya Jana,[a] Petra Lippmann,[b] Ingo Ott,[b] and Neeladri Das[a]*

[a]Department of Chemistry, Indian Institute of Technology Patna, Bihta 801 106, Bihar, India
[b]Institute of Medicinal and Pharmaceutical Chemistry, Technische Universität Braunschweig, Beethovenstraße 55, Braunschweig 38106, Germany
*E-mail: neeladri@iitp.ac.in; neeladri2002@yahoo.co.in

Received July 17, 2018
DOI 10.1002/jhet.3547
Published online 00 Month 2019 in Wiley Online Library (wileyonlinelibrary.com).

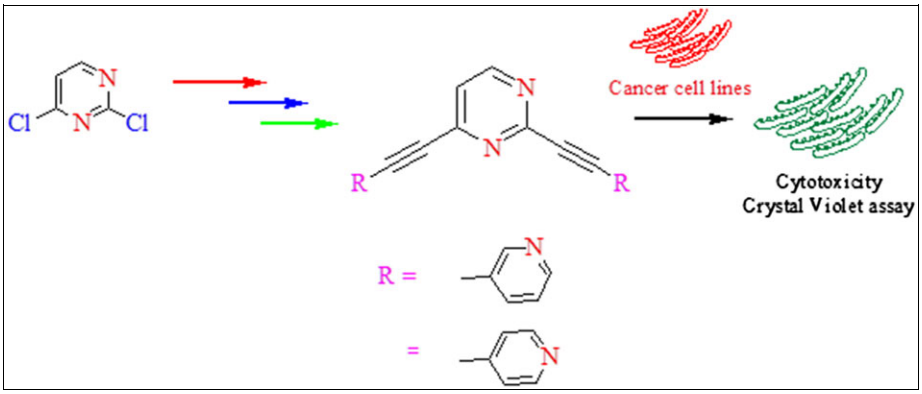

Incorporation of heterocyclic pyrimidine or pyridine motifs is common in the drug design for various therapeutic applications. Herein, we describe the facile synthesis of two molecules containing both pyrimidine and pyridine scaffolds. A variety of analytical techniques (multinuclear NMR, Fourier transform infrared, and mass spectrometry analyses) confirmed the purity of these molecules. In pristine form, their potential as antitumor drugs was screened by investigating their cytotoxicity against various cell lines (cancerous and normal cells). Experimental results confirmed that the two molecules exhibited cell growth inhibition at very low concentrations. This was evident from their IC_{50} values that are in the range of 0.45–2.20 μM.

J. Heterocyclic Chem., **00,** 00 (2019).

INTRODUCTION

Pyridine and pyrimidine are two popular six-membered heterocycles that are known for more than a century and have been investigated by numerous research groups [1–4]. Derivatives of pyridine have been used as pharmaceuticals [5], pesticides [6], and manufacture of other products [7]. The pyrimidine moiety, on the other hand, is ubiquitous because it is an integral part of DNA and RNA of living organisms [8]. Furthermore, the pyrimidine motif is also found in many natural products [8,9] (such as marine alkaloids) and used in therapeutics [10]. Thus, there is a considerable research interest in the development of new molecules that contain these heterocycles, and subsequently, these are screened for their biological interactions, especially cytotoxicity against various cancer cell lines [11]. The ethynyl functional group (–C≡C–) is another important structural motif that has been incorporated particularly in organometallic complexes of Au(I) and Pt(II) metal ions, and the resulting compounds have been studied as "inorganic" therapeutics agents for anticancer drugs [12]. Considering the diverse biological activities of these three structural motifs reported in literature, we were motivated to design unique molecules that bear all the three aforementioned units, namely, pyrimidine, pyridine, and ethynyl functional groups. Thereafter, we were curious to study their cytotoxicity with respect to various cancer cell lines. Interestingly, these newly synthesized molecules have shown quite strong cell growth inhibitory effects against various cancers cell lines (HT-29, MCF-7, and MDA-MB-231). The obtained data are comparable or in some case much better than the data previously reported in literature with compounds bearing pyrimidine, pyridyl, or ethynyl units (in organic compound or in metal–organic compound) [13].

RESULTS AND DISCUSSION

Synthesis and characterization of molecules containing pyrimidine and pyridine units (2 and **3**). Cross-coupling reaction is a powerful tool to join various structural motifs *via* C–C bonds. Sonogashira reaction is one such cross-coupling reaction, and it is an efficient synthetic protocol for introducing an ethynyl moiety on aryl compounds [14]. In the past, this reaction was used to synthesize bis- and tris(arylethylnyl)pyrimidine oligomers

Scheme 1. Synthesis of 2,4-diethynylpyrimidine.

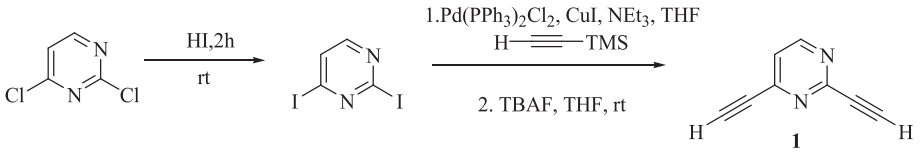

[15]. In the present work, 2,4-diethynylpyrimidine was obtained from 2,4-dichloropyrimidine *via* the formation of 2,4-diidopyrimidine (Scheme 1), because the yield of Sonogashira coupling reaction between 2,4-dichloropyrimidine and trimethylsilylacetylene was low (25%). The reaction between 2,4-diidopyrimidine and trimethylsilylacetylene was a more efficient cross-coupling reaction (yield >85%). Therefore, 2,4-dichloropyrimidine was first converted into its diiodo derivative, and this was subsequently reacted with ethynyltrimethylsilane to yield 2,4-diethynylpyrimidine (**1**) as shown in Scheme 1.

To obtain the desired molecules (bearing both pyrimidine and pyridine motifs), **1** was subjected to another Sonogashira cross-coupling reaction (Scheme 2) with either 4-iodopyridine or 3-iodopyridine in the presence of Pd(II) catalyst and Cu(I) as co-catalyst. These reactions yielded **2** and **3** respectively in reasonably high yields (>80%). Compounds **2** and **3** were obtained as white solids that are stable in air/moisture and have high solubility in common organic solvents such as acetone, halogenated solvents, methanol, and tetrahydrofuran.

Spectroscopic properties of 2 and 3. These molecules (**2** and **3**) were characterized by FT-IR and NMR (^{1}H and ^{13}C) spectroscopy, mass spectrometry, and elemental analyses. FT-IR spectra of **2** and **3** show presence of a strong band at 2216 and 2221 cm^{-1} ($\upsilon_{C\equiv C}$ str.), respectively, indicating the presence of the ethynyl functional group in the final product (Figs. S5 and S6, respectively). In the ^{1}H NMR spectrum of **2** (Figs. 1 and S1), the two chemically inequivalent protons of the pyrimidine ring appear as doublets in the range 8.83–8.82 and 7.52–7.50 ppm. The two pendant pyridine rings are chemically inequivalent. Therefore, two sets of signals are observed for α-pyridyl and β-pyridyl protons in **2** in the range of 8.70–8.67 and 7.51–7.47 ppm (Fig. 1). Similarly, in case of **3**, signals corresponding to the two protons of pyrimidine ring appear as doublets, while the four chemically nonequivalent protons present in each pendant pyridine appear as distinctly different set of signals (Fig. S3). The ^{13}C{^{1}H} NMR spectrum of both **2** and **3** exhibited all the characteristic peaks corresponding to pyrimidine, pyridine, and ethynyl units in expected region (Figs S2 and S4, respectively). Further, formation and purity of **2** and **3** were also confirmed from its mass spectrometric analysis (Figs. S7 and S8, respectively).

The absorbance maximum of compound **2** is centered at 275 nm, whereas a slightly red-shifted absorbance peak was observed for **3** with a maximum at 295 nm in dichloromethane (conc. = 10^{-5} M) at 298 K (Fig. 2). The difference in λ_{max} values of these compounds can be attributed to the difference in the position of pyridine N atom in these two molecules.

X-ray crystallographic analysis of 2. Single crystals of **2**, suitable for X-ray diffraction, were obtained by slow evaporation of its methanol solution at ambient temperature. Compound **2** crystallizes in the orthorhombic space group *Pnn2*. Crystallographic data and refinement parameters for **2** are listed in Table 1. The molecular structure with the numbering scheme is shown

Scheme 2. Synthesis of pyrimidine-based organic molecules **2** and **3**.

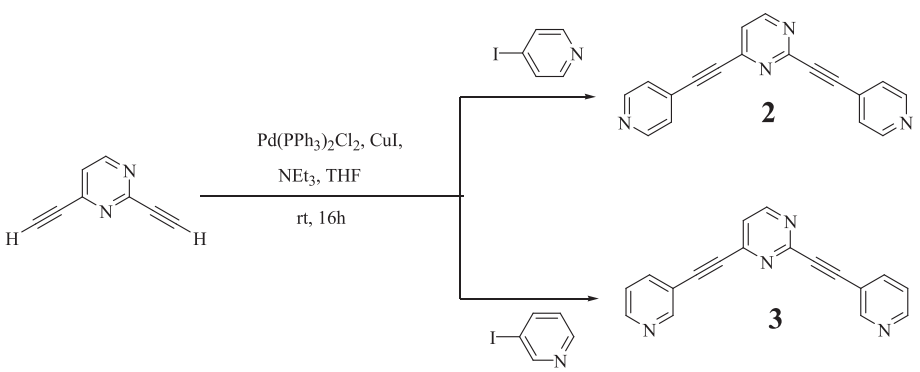

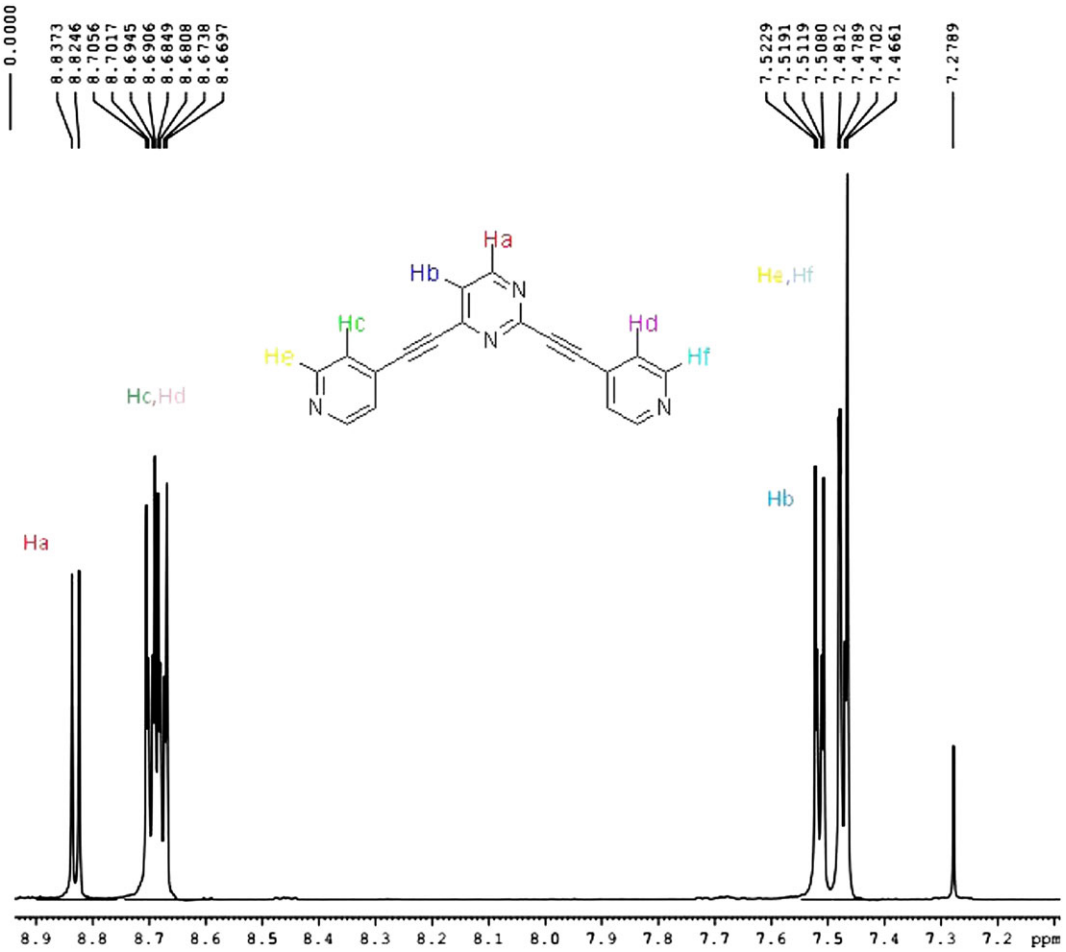

Figure 1. ^{1}H NMR spectrum of **2**. [Color figure can be viewed at wileyonlinelibrary.com]

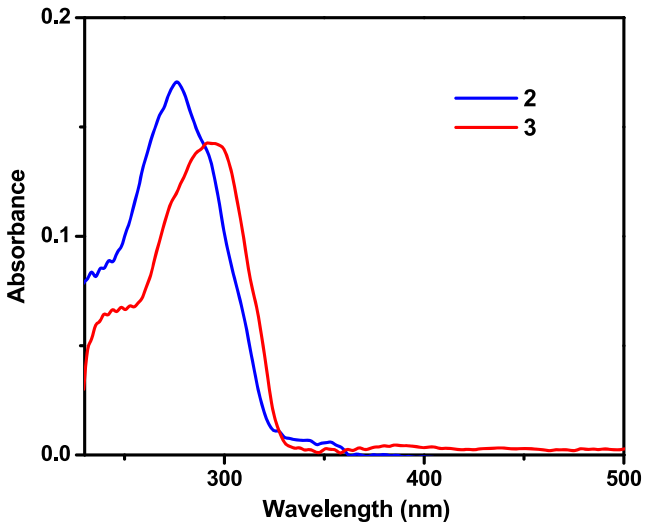

Figure 2. UV absorbance spectra of **2** and **3** recorded in DCM (conc. = 10^{-5} M) at 298 K. [Color figure can be viewed at wileyonlinelibrary.com]

in Fig. 3. The two pendent 4-ethynylpyridine moieties are not in the same molecular plane that contains the central pyrimidine ring, as evident from Fig. 3b.

Crystallographic analysis reveals that all three nitrogen atoms (N1, N2, and N3) have intermolecular interactions with the neighboring molecules *via* "hydrogen bridges."

Table 1

Crystallographic data and refinement parameters for **2**.

	2
Formula	$C_{18}H_9N_4$
Mw ($gmol^{-1}$)	281.29
Temp (K)	100 (2)
λ (Mo Kα) (Å)	0.71073
Crystal system	Orthorhombic
Space group	*Pnn2*
a (Å)	30.395 (12)
b (Å)	3.8049 (15)
c (Å)	6.058 (2)
α (°)	90
β (°)	90
γ (°)	90
V ($Å^3$)	700.6 (5)
Z	4
D_{calc} (g/cm^3)	1.333
μ (mm^{-1})	0.083
F(000)	290.0
Collected reflections	9552
Unique reflections	1556
Max and min trans	0.7404, 0.5566
Goodness of fit on F^2	1.040
R_1 [$I > 2\sigma(I)$][a]	0.0431
wR_2 (all data)[b]	0.1107
CCDC number	1565950

[a] $R_1 = \sum\left||F_o| - |F_c|\right| / \sum|F_o|$.
[b] $wR_2 = \{\sum[w(F_o^2 - F_c^2)^2] / \sum[w(F_o^2)^2]\}^{1/2}$.

The corresponding bond parameter for such intermolecular interactions (N···H–C) is listed in Table 2. The N···H distances are in the range 2.27–2.80 Å, while the C···N distances lie in between 3.35 and 3.70 Å. Based on literature reports, these interactions may be termed as "weak hydrogen bonds" because in each case, an H atom bridges two atoms of relatively low electronegativity [16]. In one of the instances, the linear geometry of the three atoms (C–H···N) supports this interaction to be termed as a weak hydrogen interaction with more certainty than the other two. These weak H-bonding interactions, present in the crystal lattice of **2**, are shown in Figure S9. In addition to such electrostatic interactions involving H bridges, there are evidences of π–π interactions between neighboring molecules of **2**. The term "π–π interactions" has been applied in event of stacking of aromatic rings having their respective

Table 3

Cytotoxicity as IC_{50} values (μM) in several cell lines with standard errors as superscripts.

	HT-29	MCF-7	MDA-MB-231	RC-124
2	$0.80^{\pm0.10}$	$0.56^{\pm0.08}$	$0.62^{\pm0.19}$	$0.44^{\pm0.08}$
3	$2.12^{\pm0.21}$	$1.37^{\pm0.22}$	$1.27^{\pm0.39}$	$1.27^{\pm0.38}$

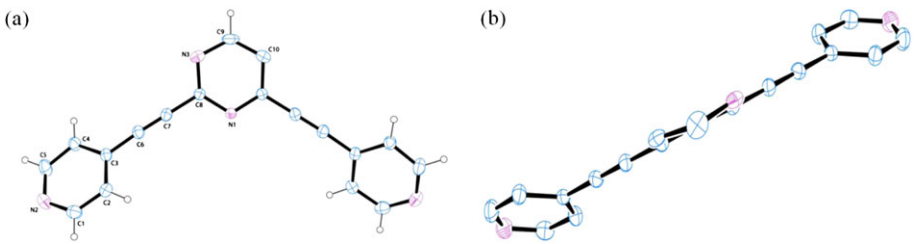

Figure 3. (a) ORTEP presentation of **2** (30% thermal ellipsoid), (b) viewing along the plane containing the central pyrimidine ring. [Color figure can be viewed at wileyonlinelibrary.com]

Table 2

Selected weak H-bond parameters observed in **2**.

D–H···A	D–H (Å)	H···A (Å)	D···A (Å)	<D–H–A (°)	Symmetry
C2–H2···N3	1.080	2.800	3.697	140.39	$x,+y+1,+z-1$
C5–H5···N2	1.080	2.486	3.392	140.79	$-x+1/2+1,+y-1/2,+z+1/2$
C9–H9···N1	1.080	2.270	3.350	180.00	$x,+y,+z+1$

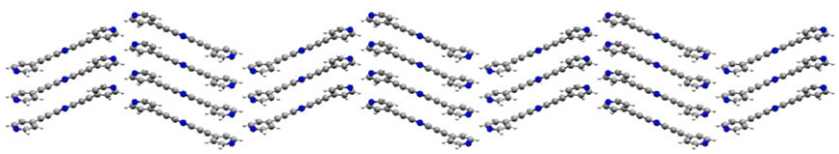

Figure 4. Packing view of **2** along *c*-axis. [Color figure can be viewed at wileyonlinelibrary.com]

molecular planes separated by 3.3–3.8 Å [17]. In the present case, the pyridine rings of neighboring molecules have interplanar separation of 3.80 Å. The packing view of **2** is shown in Fig. 4.

Cytotoxicity of pyrimidine–pyridine mixed molecules 2 and **3**. The cell growth inhibitory effects have been studied in three different types of cancer cell lines, namely, HT-29 (colon carcinoma cells), MCF-7, and MDA-MB-231 (breast cancer cells). Results (Table 3) were compared with the effect on non-cancerous RC-124 kidney cell line that was used as a reference to check for possible tumor selectivity. Both compounds (**2** and **3**) have demonstrated good cytotoxicity (0.50- to 2.20-μM range) against all three cancer cell lines. Comparison between **2** and **3** indicates a certain trend. The former (**2**) is more effective against cancer cell proliferation having lower IC_{50} values (in the range of 0.56–0.80 μM) than the latter (**3**). This result indicates that a subtle change in the structure causes a marked change in the activity of the molecule against carcinoma cell lines. In addition to the observed antiproliferative effects with respect to cancer cell lines, the two compounds (**2** and **3**) also triggered IC_{50} value in similar concentration range for non-tumor (RC-124 human kidney) cell lines. This implies that **2** and **3** do not show any selectivity for the carcinoma cells in the same doses/concentration range. Nevertheless, the cytotoxicity of these pyridine/pyrimidine-based molecules against these carcinoma cell lines is superior in comparison with several organic ligands as well as their metal complexes such as N-heterocyclic carbenes and their organometallic Au(I) [18], Ru(II), Rh(I), and Cu(I) [19] N-heterocyclic carbenes complexes.

CONCLUSION

Herein, we have reported the synthesis of two new molecules having the unique feature of possessing three motifs that are reported to have a wide spectrum of biological activities. The three motifs are pyridine, pyrimidine, and ethynyl. Compounds have been obtained in reasonable high yields using metal-catalyzed Sonogashira cross-coupling reactions. These nitrogen-rich molecules (**2** and **3**) were thoroughly characterized by FT-IR, multinuclear NMR spectroscopy, ESI-TOF-MS spectrometry, and elemental analyses. Compound **2** was also structurally characterized by single-crystal X-ray diffraction. Considering the anticancer potencies of pyridine-based or pyrimidine-based molecules, it was our curiosity to investigate the anticancer activity of the two newly synthesized molecules. Consequently, **2** and **3** were tested against three different cancer cell lines (HT-29, MCF-7, and MDA-MB-231). The cytotoxic activity results revealed that both are active (IC_{50} values <2.2 μM) against the tested colon and breast carcinoma cells. Our studies also show that the molecule with 4-pyridyl pendant groups is more active (IC_{50} values <0.9 μM) against all three carcinoma cell lines suggesting a strong structure–activity relationship. This work motivates others and us to study pharmacology of these and similar heterocyclic compounds in detail in near future.

EXPERIMENTAL

General details. All chemicals and anhydrous solvents used in the present work were purchased from commercial sources and used without further purification. 2,4-Diethynylpyrimidine was prepared following experimental protocol reported literature [15]. FTIR spectra were recorded in a PerkinElmer spectrum 400 FT-IR spectrophotometer. ^1H and $^{13}C\{^1H\}$ NMR spectra were recorded on a Bruker 400-MHz spectrometer. Elemental analyses were carried out using an Elementar vario Micro Cube elemental analyzer. HRMS (ESI-MS) analysis was performed using a Bruker Impact ESI-Q-TOF system.

Synthesis of 2 and **3**. 2,4-Diethynylpyrimidine (50 mg, 0.390 mmol), iodopyridine (159.90 mg, 0.78 mmol) (4-idopyridine for **2** and 3-idopyridine for **3**), Cu(I) (7.4 mg, 0.03 mmol), and bis(triphenylphosphine) palladium(II) dichloride (27.37 mg, 0.03 mmol) were charged in a 50-mL Schlenk flask in the glove box. Subsequently, 10-mL dry THF and freshly distilled triethylamine (0.5 mL, 1.56 mmol) were added under nitrogen. The reaction mixture was stirred overnight at room temperature. Subsequently, the dark brown reaction mixture was filtered through a bed of celite. The filtrate obtained was evaporated to dryness on a rotary evaporator to yield the crude product that was purified by column chromatography on neutral alumina by eluting with 35% ethyl acetate in hexane to isolate the desired products (**2** and **3**) as off-white solids.

2,4-Bis-pyridin-4-ylethynyl-pyrimidine (2). Yield: 0.095 g, 86%; mp 153–158°C; ^1H NMR (400 MHz, $CDCl_3$): δ 8.83–8.82 (d, 1H, J = 4 Hz Ar–H), 7.52–7.51 (d, 1H, J = 4 Hz, Ar–H), 8.70–8.66 (m, 4H, Ar–H), 7.50–7.46 (m, 4H, Ar–H). $^{13}C\{^1H\}$ NMR ($CDCl_3$, 100 MHz): δ 157.9, 152.8, 150.5, 150.1, 150.0, 129.2, 128.9, 126.0, 125.8, 122.5, 91.8, 90.8, 89.3, 84.9, IR (ATR): 3024, 2920, 2851, 2216, 1734, 1586, 1401, 1383, 1309, 1187, 1112, 996, 951, 869, 811 cm^{-1}. *Anal*. Calcd for $C_{18}H_{10}N_4C$, 76.58; H, 3.57; N, 19.85. Found: C, 76.71; H, 3.66; N, 19.92. HRMS (ESI, *m/z*): calculated for $C_{18}H_{10}N_4$ ($[M + H]^+$): 283.10; found: 283.10. CCDC 1565950.

2,4-Bis-pyridin-3-ylethynyl-pyrimidine (3). Yield: 0.097 g, 88%; mp 165–170°C; ^1H NMR (400 MHz,

$CDCl_3$): δ 8.91–8.90 (m, 1H, Ar–H), 8.86–8.86 (m, 1H, Ar–H), 8.80–8.79 (d, J = 4 Hz, 1H, Ar–H), 8.66–8.63 (m, 2H, Ar–H), 7.97–7.90 (m, 2H, Ar–H), 7.44–7.43 (d, J = 4 Hz, 1H, Ar–H), 7.37–7.32 (m, 2H, Ar–H). $^{13}C\{^1H\}$ NMR ($CDCl_3$, 100 MHz): δ 157.7, 153.1, 153.0, 152.9, 150.8, 150.3, 150.0, 139.5, 139.3, 123.2, 123.1, 122.0, 118.5, 118.2, 91.1, 90.5, 89.0, 84.8. IR (ATR): 3030, 2920, 2857, 2221, 1545, 1470, 1412, 1320, 1187, 1187, 1124, 1019, 945, 846, 800, 702 cm^{-1}. *Anal*. Calcd for $C_{18}H_{10}N_4$: C, 76.58; H, 3.57; N, 19.85. Found: C, 76.83; H, 3.76; N, 19.98. HRMS (ESI, *m/z*): calculated for $C_{18}H_{10}N_4$ ($[M + H]^+$): 283.10; found: 283.10.

Single-crystal structure determination. A suitable single crystal of **2** was carefully selected under a polarizing microscope and mounted on a crystal mounting loop after coating with paratone oil. Single-crystal data were collected on a Bruker D8 Quest diffractometer equipped with an Oxford Cryostream low-temperature device and a fine-focus sealed-tube X-ray source (Mo-Kα radiation, λ = 0.71073 Å, graphite monochromated) operating at 50 kV and 30 mA. The unit cell measurement, data collection (φ and ω scan), integration, scaling, and absorption corrections for the crystal were performed using Bruker Apex II software [20]. The structure was solved using direct method followed by full matrix least square refinements against F^2 (all data HKLF 4 format) using SHELXTL [21]. A multiscan absorption correction, based on equivalent reflections, was applied to the data. Anisotropic refinement was used for all non-hydrogen atoms. Hydrogen atoms were placed in appropriate calculated positions.

Cell culture and cytotoxicity assay. HT-29 colon carcinoma cells, MDA-MB-231 breast cancer cells, MCF-7 breast carcinoma cells were maintained in Dulbecco's Modified Eagle Medium (4.5 g/L (D)-glucose, L-glutamine, pyruvate), which was supplemented with gentamycin (50 mg/L)and fetal bovine serum superior, standardized (Biochrom GmbH, Berlin) (10% v/v), and were passaged once a week. Determination of antiproliferative effects involved the following protocol described by Ott and coworkers [22]. One hundred microliters of cells (HT-29: 2565 cells/mL, MCF-7: 4840 cells/mL, MDA-MB-231: 4120 cells/mL, or RC-124: 1460 cells/mL) were seeded into the wells of 96-well plates and incubated at 37°C/5% CO_2 atmosphere) for 48 h (HT-29) or 72 h (MCF-7, MDA-MB-231, and RC-124). After the incubation period, the cells in one plate were fixed by addition of 100 µL of a 10% glutaraldehyde solution, and the plate was stored at 4°C (t_0 plate). Stock solutions of the compounds (**2** and **3**) in DMSO were freshly prepared and diluted with the respective cell culture medium to graded concentrations (final concentration of DMSO: 0.1% v/v). In the remaining plates, the medium was replaced by different concentrations of the compound in cell culture medium (six wells for each concentration). Twelve wells of each plate were treated with a solution of 0.1% DMF in cell culture medium (untreated control). Subsequently, the plates were incubated at 5% CO_2 and 37°C for 72 h (HT-29) or 96 h (MDA-MB-231). After exposure to the **2** and **3**, the medium was removed, and the cells were treated with 100 µL of a 10% glutaraldehyde solution. Afterwards, the cells of all plates were washed with 180-µL PBS and stained with 100 µL of a 0.02% crystal violet solution for 30 min. The crystal violet solution was removed, and the plates were washed with water and dried. A volume of 180 µL of ethanol 70% was added to each well, and after 3–4 h of gentle shaking, the absorbance was measured at 595 nm in a microplate reader (Victor X4, PerkinElmer). The mean absorbance value of the t_0 plate was subtracted from the absorbance values of all other absorbance values. The IC_{50} values were calculated as the concentrations reducing the cellular proliferation in comparison with the untreated control by 50% and are given as the means and errors of three independent experiments.

Acknowledgments. N. D. thanks Indian Institute of Technology (IIT) Patna for laboratory facility and DAAD [for a "Forschungsaufenthalt" award Research Stays for University Academics and Scientists, 2018 (57378441)]. K. S. and A. J. thank UGC, New Delhi, India, for a Research Fellowship. The authors acknowledge SAIF-Panjab University for providing NMR spectroscopy facilities. The authors also acknowledge SAIF-IIT Patna for providing ESI-MS and XRD facilities.

REFERENCES AND NOTES

[1] Atwal, K. S.; Rovnyak, G. C.; O'Reilly, B. C.; Schwartz, J. J Org Chem 1989, 54, 5898.

[2] Sharma, V.; Chitranshi, N.; Agarwal, A. K. Int J Med Chem 2014, 202784 31.

[3] Toledo-Sherman, L. M.; Prime, M. E.; Mrzljak, L.; Beconi, M. G.; Beresford, A.; Brookfield, F. A.; et al. J Med Chem 2015, 58, 1159.

[4] Supaluk, P.; Ratchanok, P.; Apilak, W.; Nujarin, S.; Veda, P.; Somsak, R.; Virapong, P. Mini Rev Med Chem 2017, 17, 869.

[5] Amr, A. E.-G. E.; Al-Omar, M. A.; Abdalla, M. M. J Comput Theor Nanosci 2016, 13, 7351.

[6] Bakhite, E. A.; Abd-Ella, A. A.; El-Sayed, M. E. A.; Abdel-Raheem, S. A. A. J Saudi Chem Soc 2017, 21, 95.

[7] Goetz, A. E.; Garg, N. K. Nat Chem 2012, 5, 54.

[8] (a) Engelhart, A. E.; Hud, N. V. C. S. H. Perspect Biol 2010, 2, a002196; (b) Newman, D. J. J Med Chem 2008, 51, 2589.

[9] Forche Asobo, P.; Wahe, H.; Mbafor, J. T.; Nkengfack, A. E.; Fomum, Z. T.; Sopbue, E. F.; Dopp, D. J Chem Soc Perkin Trans 1 2001, 4, 457.

[10] Ceccherini, E.; Indovina, P.; Zamperini, C.; Dreassi, E.; Casini, N.; Cutaia, O.; Forte, I. M.; Pentimalli, F.; Esposito, L.; Polito, M. S.; Schenone, S.; Botta, M.; Giordano, A. J Cell Biochem 2015, 116, 856.

[11] Yu, W.; Goddard, C.; Clearfield, E.; Mills, C.; Xiao, T.; Guo, H.; Morrey, J. D.; Motter, N. E.; Zhao, K.; Block, T. M.; Cuconati, A.; Xu, X. J Med Chem 2011, 54, 5660.

[12] (a) Bhowmick, S.; Jana, A.; Singh, K.; Gupta, P.; Gangrade, A.; Mandal, B. B.; Das, N. Inorg Chem 2018, 57, 3615; (b) Singh, K.; Gangrade, A.; Bhowmick, S.; Jana, A.; Mandal, B. B.; Das, N. Front Chem 2018 6; (c) Jana, A.; Lippmann, P.; Ott, I.; Das, N. Inorg Chim Acta 2018, 471, 223.

[13] (a) Hocková, D.; Holý, A. N.; Masojídková, M.; Votruba, I. Tetrahedron 2004, 60, 4983; (b) Bourderioux, A.; Nauš, P.; Perlíková, P.; Pohl, R.; Pichová, I.; Votruba, I.; Džubák, P.; Konečný, P.; Hajdúch, M.; Stray, K. M.; Wang, T.; Ray, A. S.; Feng, J. Y.; Birkus, G.; Cihlar, T.; Hocek, M. J Med Chem 2011, 54, 5498; (c) McIntyre, N. A.; McInnes, C.; Griffiths, G.; Barnett, A. L.; Kontopidis, G.; Slawin, A. M. Z.; Jackson, W.; Thomas, M.; Zheleva, D. I.; Wang, S.; Blake, D. G.; Westwood, N. J.; Fischer, P. M. J Med Chem 2010, 53, 2136; (d) Pierroz, V.; Joshi, T.; Leonidova, A.; Mari, C.; Schur, J.; Ott, I.; Spiccia, L.; Ferrari, S.; Gasser, G. J Am Chem Soc 2012, 134, 20376.

[14] (a) Touzé, E.; Gohier, F.; Dabos-Seignon, S.; Breton, T.; Cougnon, C. Synth Met 2019, 247, 37; (b) Wang, S.; Gao, Y.; Shen, S.; Wen, H.; Cui, H. Molecules 2018, 23, 154; (c) Corr, M. J.; Sharma, S. V.; Pubill-Ulldemolins, C.; Bown, R. T.; Poirot, P.; Smith, D. R. M.; Cartmell, C.; Abou Fayad, A.; Goss, R. J. M. Chem Sci 2017, 8, 2039.

[15] Achelle, S.; Ramondenc, Y.; Dupas, G.; Plé, N. Tetrahedron 2008, 64, 2783.

[16] Desiraju, G. R. Acc Chem Res 2002, 35, 565.

[17] Janiak, C. J Chem Soc Dalton Trans 2000 3885.

[18] Schmidt, C.; Karge, B.; Misgeld, R.; Prokop, A.; Franke, R.; Brönstrup, M.; Ott, I. Chem A Eur J 2017, 23, 1869.

[19] Streciwilk, W.; Terenzi, A.; Misgeld, R.; Frias, C.; Jones Peter, G.; Prokop, A.; Keppler Bernhard, K.; Ott, I. Chem Med Chem 2017, 12, 214.

[20] Apex2, Version 2 User Manual, M86-E03078; Bruker Analytical X-ray Systems: Madison, WI, 2010.

[21] Sheldrick, G. M. SHELXTL Program for the Solution of Crystal of Structures; University of Gottingen: Gottingen, Germany, 1993.

[22] (a) Rubbiani, R.; Schuh, E.; Meyer, A.; Lemke, J.; Wimberg, J.; Metzler-Nolte, N.; Meyer, F.; Mohr, F.; Ott, I. Med Chem Commun 2013, 4, 942; (b) Meyer, A.; Gutiérrez, A.; Ott, I.; Rodríguez, L. Inorg Chim Acta 2013, 398, 72.

SUPPORTING INFORMATION

Additional supporting information may be found online in the Supporting Information section at the end of the article.